



Synthesis and application of visual AIE fluorescent probe for lipid droplets in vivo

Lei Wu, Bin Li, Yan Deng, Jieyu Zhou, Guangyao Shi, Yiheng Li, Xiaoqing Wang, Shaoping Wu, Yongmin Zhang, Jianli Li

► To cite this version:

Lei Wu, Bin Li, Yan Deng, Jieyu Zhou, Guangyao Shi, et al.. Synthesis and application of visual AIE fluorescent probe for lipid droplets in vivo. *Dyes and Pigments*, 2023, 209, pp.110946. 10.1016/j.dyepig.2022.110946 . hal-03865413

HAL Id: hal-03865413

<https://hal.sorbonne-universite.fr/hal-03865413>

Submitted on 22 Nov 2022

HAL is a multi-disciplinary open access archive for the deposit and dissemination of scientific research documents, whether they are published or not. The documents may come from teaching and research institutions in France or abroad, or from public or private research centers.

L'archive ouverte pluridisciplinaire **HAL**, est destinée au dépôt et à la diffusion de documents scientifiques de niveau recherche, publiés ou non, émanant des établissements d'enseignement et de recherche français ou étrangers, des laboratoires publics ou privés.

Synthesis and application of visual AIE fluorescent probe for lipid droplets *in vivo*

Lei Wu^{a, §}, Bin Li^{a, §}, Yan Deng^a, Jieyu Zhou^a, Guangyao Shi^a, Yiheng Li^a, Xiaoqing Wang^b, Shaoping Wu^{a, *}, Yongmin Zhang^{a, c}, Jianli Li^b

^a School of Pharmacy, Key Laboratory of Resource Biology and Biotechnology in Western China, Ministry of Education, Biomedicine Key Laboratory of Shaanxi Province, Northwest University, 229 Taibai Road, Xi'an, Shaanxi, 710069, P. R. China.

^b Key Laboratory of Synthetic and Natural Functional Molecule Chemistry of Ministry of Education, College of Chemistry & Materials Science, Northwest University, Xi'an, Shaanxi, 710127, P. R. China.

^c Sorbonne Université, CNRS, Institut Parisien de Chimie Moléculaire, UMR 8232, 4 place Jussieu, 75005, Paris, France.

[§] These authors contributed equally to this work.

* Tel.: +86 029 88304569; Fax: +86 029 88304569. E_mail: wushaoping@nwu.edu.cn

1. Introduction

Lipid droplets (LDs) are subcellular organelle that reposit neutral lipid in cells and play a key role in many physiological activities, for instance lipid consumption and preservation, protein production, membrane stability as well as dynamic regulation of signal transduction [1-2]. It was reported that metabolic diseases, such as diabetes, obesity and cardiovascular disease were closely related to elevated lipid store in LDs [3]. Accordingly, it is of great significance to exploit biological fluorescent probes with excellent optical capabilities for LDs imaging for investigating their physiological function and developing a tool for early diagnosis of related diseases.

Naphthalenone, an aromatic conjugated system containing double rings, is an important chemical raw material and pharmaceutical intermediate. Because of its excellent optical properties and easy synthesis, naphthalenone derivatives have huge potential in the synthesis of fluorescent probes [4]. Fluorescent probes have attracted extensive attention by reason that their adjustable emission color, excellent luminescence performance and easy modification [5]. In recent years, many fluorescent probes have been reported for the specific exploration of LDs, such as Nile red and BODIPY493/503, however in aggregated state these probes experience aggregation-caused quenching (ACQ) effects due to intermolecular π - π stacking [6]. On the side,

commercially available probes for detecting LDs exposed poor photobleaching resistance and low signal-to-noise ratio, which limit their adhibition in biological imaging. During the past years, a large amount of aggregation-induced emission (AIE) luminogens have been reported as potential fluorescent probes for organism image [7]. Unlike the strong emission of ACQ in the organic solvent, AIEgens have little or no emission in the solution as the excited state energy is expended in the intramolecular rotation (RIR) [8]. However, once the molecule occurs aggregation process, the intramolecular rotation is effectively limited, and the energy is released in the form of radiative transition, resulting in a significant increase in fluorescence intensity of the aggregated state. Because AIEgens have good luminescence performance and high signal-to-noise ratio, which make up for the shortcomings of ACQ-active luminogens, their application value in biological imaging [9], photoelectric devices [10], information storage components [11] and other fields have attracted extensive attention of researchers.

In this study, we found that there was a significant AIE effect in these luminescent materials when the intramolecular rotation of the excited state was limited. By introducing different electron-absorbing groups, the aggregation emission of the derivatives changed from 540 nm to 608 nm. This phenomenon was investigated by dynamic light scattering and theoretical calculation. The consequences revealed that the twisted configuration and condensed state effective RIR should lie behind the AIE effects of **CMDP** derivatives. Because of their excellent biocompatibility and appropriate lipophilicity, **CMDP-CN** and **CMDP-NO₂** can be used as luminogens for

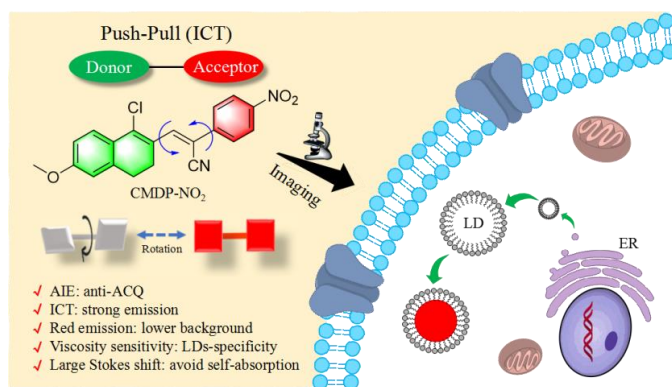


Fig. 1. Structure and rationale of **CMDP** derivatives for lipid droplet detection.

particular detection of intracellular lipid droplets and internal imaging of zebrafish yolk liposomes (**Fig. 1**).

2. Experimental section

2.1. General methods

All reactants and solvents were obtained directly from the appropriate suppliers without further purification. A Hitachi F-7000 fluorescence spectrophotometer was used to collect fluorescence spectra. A Shimadzu UV-2550 spectrophotometer was used to collect UV-vis spectral data. Laser scanning confocal fluorescence microscopy Leica TCS SP8 (Leica, Berlin, Germany) was used to collect the cell fluorescence imaging. HRMS spectra were acquired on a Bruker micrOTOF-Q II mass spectrometer (Bruker Daltonics Corp., USA) in electrospray ionization (ESI) mode. JNM-ECZ400S spectrometer (JEOL, Tokyo, Japan) was used to record ^1H and ^{13}C NMR spectra operating at 400 and 100 MHz, respectively.

2.2. General procedure for the spectral measurements

The stock solution of **CMDP** derivatives (1.0 mM) was prepared in ACN. For representative AIE optical measurements, the test solution was prepared by adding 25 μL (1.0 mM) to different acetonitrile/water mixtures with different water fractions (f_w). After being stored at room temperature (25 $^\circ\text{C}$) for 5 min, the fluorescence or absorption spectra were determined.

2.3. Fluorescence imaging

Co-localization experiments. The HepG2 cells were firstly incubated with 5.0 μM of **CMDP** derivatives and BODIPY493/503 (500 nM) at 37 $^\circ\text{C}$ for 30 min. Then the cells were washed with PBS twice before imaging.

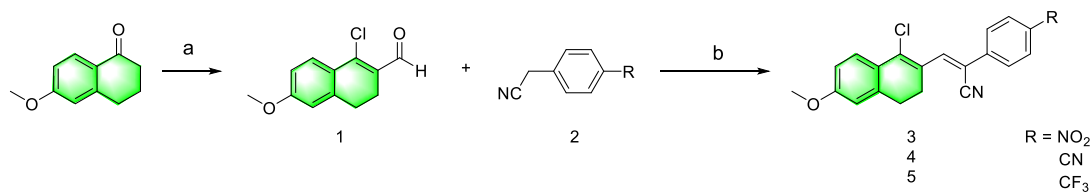
Wash-free imaging. The HepG2 cells were incubated with **CMDP** derivatives (5 μM), Nile Red (500 nM) and BODIPY493/503 (500 nM) for 30 min, respectively. After that, the cells were imaged directly using confocal microscopy without washing by PBS.

Fast-staining experiments. The HepG2 cells were washed with PBS twice. After that, the **CMDP** derivatives in DMEM medium were added to give the final concentration of 5.0 μM . Then the fluorescent images were collected over time.

Zebrafish imaging. Zebrafish embryos were incubated at 27 °C in EM culture medium. After 24~48 h incubation, PTU (75.0 μM) was added into EM culture medium to prevent the formation of melanin, which could keep the fish body optically transparency. For confocal imaging experiments, zebrafish larvae were soaked in 1.0 mL of EM containing **CMDP** derivatives (5.0 μM) for 30 min. Then the dye-stained zebrafish larvae were washed with fresh PBS solution for three times. The zebrafish larvae were anesthetized by 0.003% tricaine methane sulfonate before confocal imaging.

2.4. Synthesis

The synthesis method of **CMDP** derivatives is shown in **Scheme 1**. Firstly, Phosphorus Oxychloride and *N,N*-dimethylformamide reacted for 30 minutes, and then reacted with 6-methoxy-1-tetralone via Vilsmeier-Hacck formylation in 71.0 % yield to obtain compound **1**. Further compound **3** was obtained by condensation reaction of 4-nitrophenylacetonitrile with compound **1** in methanol in 90.1% yield. Following similar steps, compound **4** and **5** were synthesized. Specific experimental operations and data are shown in the supplementary information.



Reagents and conditions: a) POCl₃, DMF, 90°C, 5 h, 71%; b) Piperidine, MeOH, 70°C, 90 min, CMDP-NO₂: 81%; CMDP-CN: 75%; CMDP-CF₃: 50%.

Scheme 1. Synthetic routes to **CMDP** derivatives.

3. Results and discussion

3.1. Synthesis and fluorescence properties

The **CMDP** derivatives were synthesized via a simple two-step organic reaction. In order to obtain the near-infrared AIE fluorescent probe with long emission wavelength, three substituents with different absorbability were substituted in the acetonitrile structure (**Scheme 1**) with 50-81% yield.

Compound **CMDP-CF₃**, **CMDP-CN** and **CMDP-NO₂** were completely dissolved in acetonitrile (ACN), and the measured UV-vis spectra peak appeared at 383 nm, 390 nm, and 404 nm (**Fig. S1**), respectively. The absorption wavelength of gradual redshift

can put down to the orderly enhanced the intramolecular charge transfer transition from **CMDP-CF₃** to **CMDP-NO₂**. Subsequently, the fluorescent properties of **CMDP** derivatives in the aggregated state were investigated in acetonitrile/water mixtures with different water fractions (f_w). **CMDP-CN** and **CMDP-NO₂** emitted weak blue fluorescence at 540 nm and 608 nm in ACN solution, whose intensity gradually increased 104- and 40-fold by adding the poor solvent of water into ACN solution from 0 to 80% ($\Phi_f = 37\%$ and 19%), at the same time, **CMDP** derivatives showed a large stokes shift (>140 nm), which prevented the absorption of the luminescence source from and facilitated the application in bioimaging (**Table 1**). When f_w exceeded 80% the relative fluorescence intensity (I/I_0) decreases obviously due to the large size of nano-aggregates (**Fig. 2A-2D**). Furthermore, dynamic light scattering measurements confirmed that the molecular aggregation at f_w of 80%, and the particle sizes of **CMDP-CN** and **CMDP-NO₂** were 188.7 nm and 410.5 nm, respectively (**Fig. S2**). This result proved that **CMDP-CN** and **CMDP-NO₂** had special AIE behavior. However, compound **CMDP-CF₃** was non-emissive in ACN/water mixtures (**Fig. S3**).

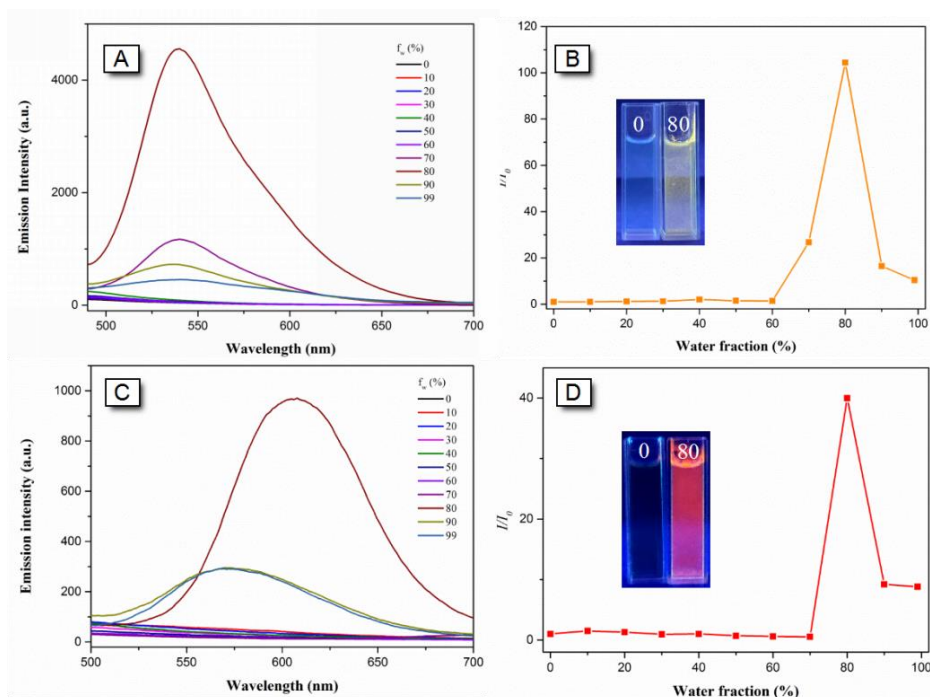


Fig. 2. Fluorescence intensity responses of **CMDP-CN** (A) and **CMDP-NO₂** (C) in ACN/water mixtures with varied f_w at room temperature. The relative fluorescence intensity of I/I_0 of **CMDP-CN** (B) and **CMDP-NO₂** (D) versus f_w . The final concentration of the probe was 20 μ M. Inset: picture of **CMDP-CN** (B) and **CMDP-NO₂** (D) in ACN/water mixtures under 365 nm UV irradiation.

Table 1 Photophysical properties of **CMDP** derivatives.

AIEgen	Solution ^a				Aggregation ^b		HOMO[eV]	LUMO[eV]	E_g [eV]
	λ_{abs}	ϵ	λ_{em}	Φ_f	λ_{abs}	Φ_f			
	[nm]	[M ⁻¹ cm ⁻¹]	[nm]	[%]	[nm]	[%]			
CMDP-CF₃	383	15649	500	0.04	390	1	-7.17	-1.97	5.20
CMDP-CN	390	15388	540	0.09	385	37	-7.17	-2.08	5.09
CMDP-NO₂	404	15784	608	0.02	380	19	-7.20	-2.33	4.87

a) In acetonitrile solution (20 μ M); b) In acetonitrile/water mixtures with f_w of 80%;

3.2. Density functional theory

Density functional theory can be used to construct the molecular geometries of **CMDP** derivatives in ground (S_0) and excited (S_1) states respectively to study their emission properties in the dissolved state. As shown in **Fig. 3A-C**, the molecular geometries of **CMDP** derivatives in S_1 state exhibited discrepancy than those in S_0 state, which was presumably because of the flexibility of intramolecular rotatable single bonds. The structural differences after optimization indicated that the structural relaxation of the excited state **CMDP** derivatives was large, which further promoted non-radiative decay. As a result, the emission of **CMDP** derivatives in the dissolved state was very weak.

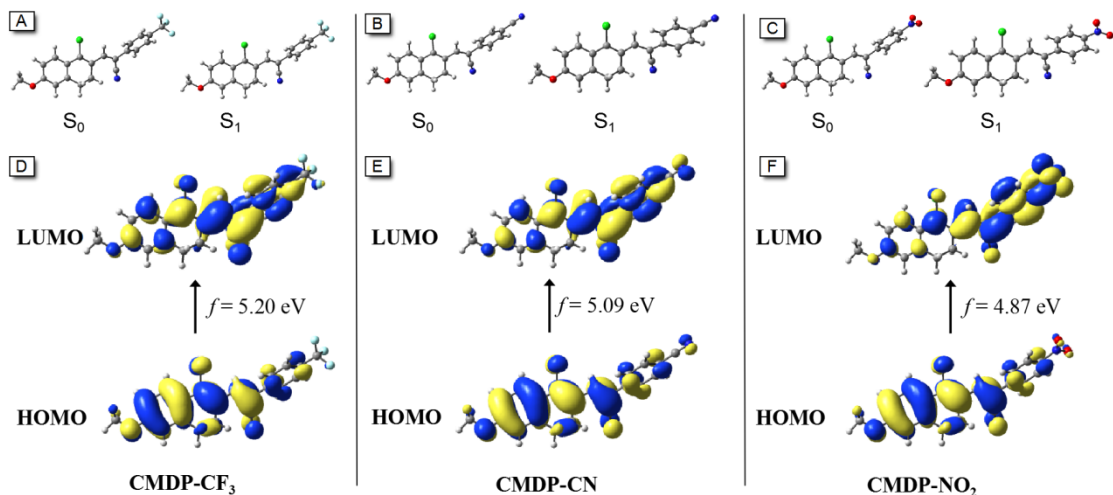


Fig. 3. Optimized structures of (A) **CMDP-CF₃**, (B) **CMDP-CN** and (C) **CMDP-NO₂** in the S_0 and S_1 states. The distributions of HOMO and LUMO molecular orbitals of (D) **CMDP-CF₃**, (E) **CMDP-CN** and (F) **CMDP-NO₂** were calculated by DFT method.

The frontier orbital distributions and energy levels of **CMDP** derivatives were

computed (**Fig. 3D-F**). HOMO was basically located in central portion and at naphthalenone group attached to methoxy-*O* atom, however LUMO was delocalized at the part containing different electricity-absorbing groups of phenylacetonitrile, which demonstrated that there was an obvious phenomenon of ICT in **CMDP-CN** and **CMDP-NO₂**. The energy levels of HOMO were computed to be -7.17 eV to -7.20 eV, while the energy levels of LUMO were -1.97 eV to -2.33 eV in the order from **CMDP-CF₃**, **CMDP-CN** and **CMDP-NO₂**. Their energy gaps between HOMO and LUMO were 5.20 eV, 5.09 eV, 4.87 eV respectively, resulting in their red-shift absorption behavior in solution (500 nm to 608 nm).

3.3. Co-localization studies

The biocompatibilities of **CMDP-CN** and **CMDP-NO₂** were further assessed by the method of MTT assay (**Fig. S4**). When the concentration of **CMDP-CN** and **CMDP-NO₂** was respectively enhanced to 10 μ M, the cell viability was still more than 85%, which exhibited they possess good biocompatibilities and no noticeable inhibitory effect was observed on HepG2 cells. Due to the internal lipophilic environment of LDs, neutral luminogens with high lipophilic properties usually accumulate in the LDs of living cells. In recent years, efforts have been made to construct fluorescent probes to detect LDs, whose molecules are shown in **Table S1** [12-21]. However, in order to optimize the application of lipid droplet probes in biological systems, some improvements are needed to reduce background fluorescence, improve signal-to-noise ratio and shorten culture time. For purpose of doing that the excellent AIE properties of **CMDP** derivatives were used as selective probes for LDs in HepG2 cells. The fluorescent bioimaging experiments of **CMDP-CN** and **CMDP-NO₂** were evaluated by co-localization experiments using the commercial LDs reagent (BODIPY 493/503) as reference. HepG2 cells were hatched with **CMDP-CN**, **CMDP-NO₂** and BODIPY493/503 for 30 min, as shown in **Fig. 4**, the strong fluorescent signals with different colors from **CMDP-CN** and **CMDP-NO₂** channel were watched, which accurately superimposed with the signals originated from BODIPY 493/503. The Pearson's coefficient was calculated to be 0.98 and 0.88 for **CMDP-CN** and **CMDP-**

NO₂, respectively, showing that **CMDP** derivatives could image LDs characteristically in living cells.

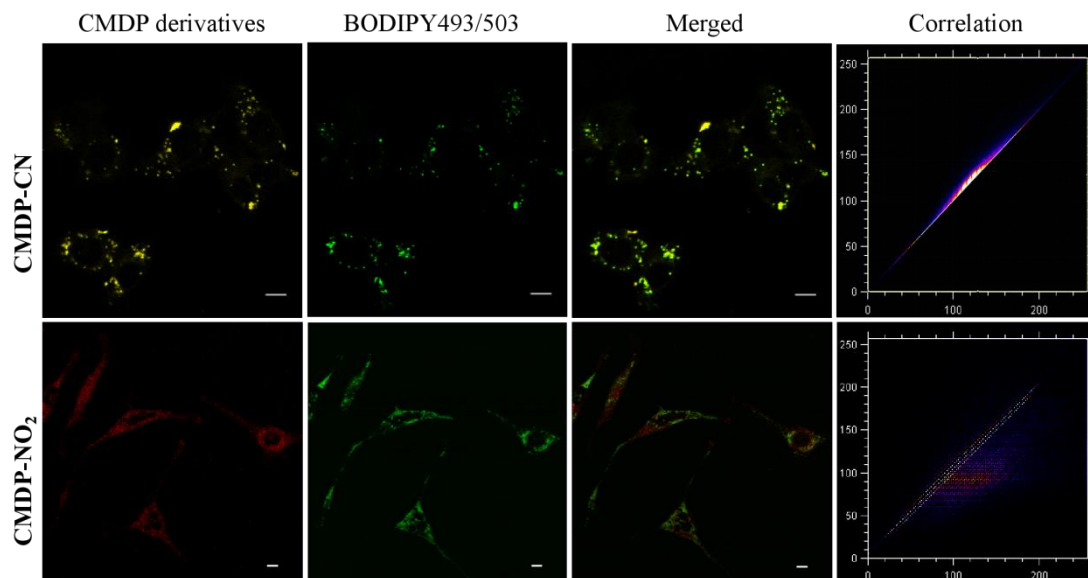


Fig. 4. Confocal fluorescence microscopic images of HepG2 cells. HepG2 cells incubated by probe **CMDP** derivatives (5.0 μ M) and BODIPY493/503 (500 nM). Scale bar: 10 μ m.

3.4. Wash-free imaging and fast-staining experiments

Non-flushing imaging of organelles can simplify the staining process and dynamically monitors the morphological changes of organelles *in situ*. Thanks to **CMDP** derivatives' individual luminescence performance in the aggregated state, we evaluated their imaging ability without washing (**Fig. 5A**). Interestingly, a strong fluorescence signal of **CMDP** derivatives was observed from LDs, which was almost indistinguishable from the rinsed image. However, the cells solidified with commercial probes BODIPY 493/503 or Nile red produced significant background interference. The high signal-to-noise ratio imaging of the unwashed **CMDP** derivatives can be attributed to the significant increase in emission when the molecule aggregates in LDs. This non-flushing imaging method not only simplifies the steps of cell imaging experiments, but also provides a feasible approach for monitoring the morphology of LDs *in situ*.

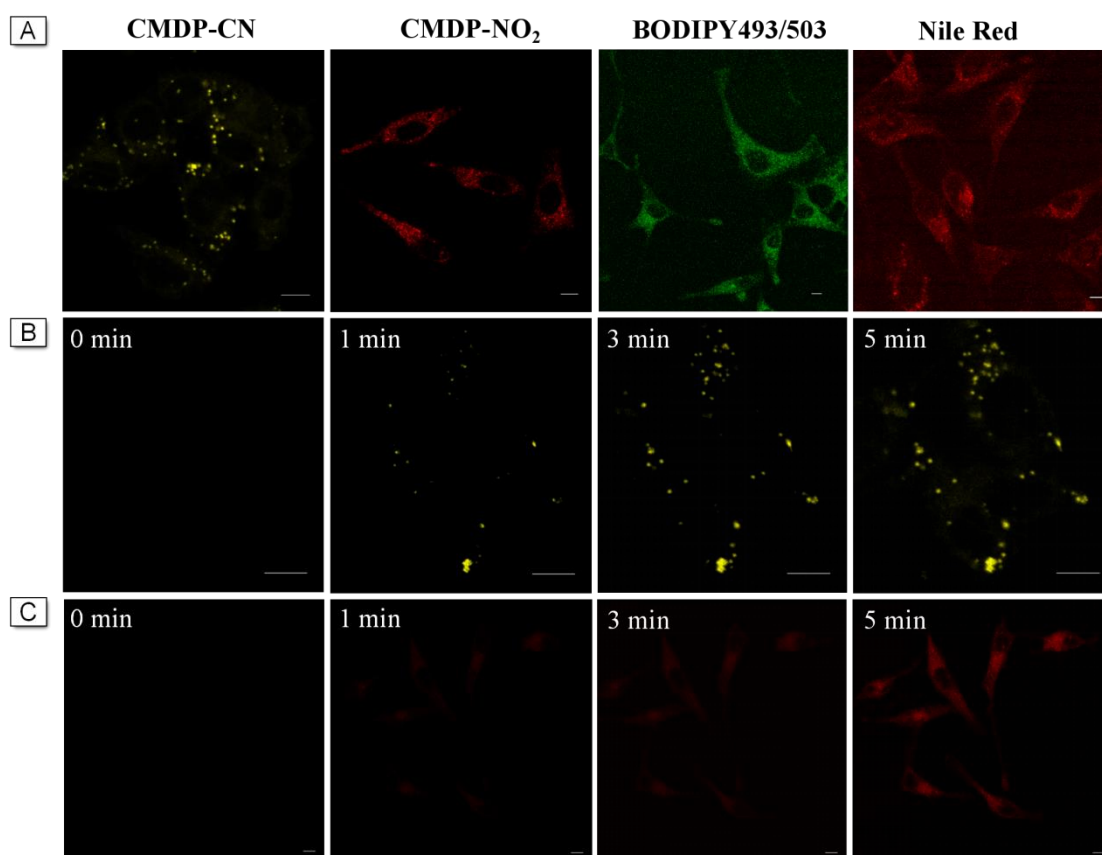


Fig. 5. (A) Confocal images of HepG2 cells stained with **CMDP** derivatives (10.0 μ M), BODIPY493/503 (200 nM) and Nile red (200 μ M) without washing. Time-dependent images of **CMDP-CN** (B) (5.0 μ M) and **CMDP-NO₂** (C) (5.0 μ M). Scale bar: 10 μ m.

The time-dependent staining rates of **CMDP-CN** and **CMDP-NO₂** on lipid droplets were studied. As shown in **Fig. 5B-C**, weak yellow and red fluorescent signals from the LDs leaded off being observed when the cells were cured with **CMDP-CN** and **CMDP-NO₂** for 0 min respectively. After 5 minutes of cell incubation, the fluorescent signals were clearly visualized, suggesting that abundant luminogens aggregated in LDs. The remarkable fluorescence increase may be ascribed to the aggregation of **CMDP** derivatives in LDs, and rotation within the molecule was effectively limited. This special fluorescent turn-on probe indicated that **CMDP** derivatives could serve as ideal candidates for tracking the LDs morphology *in situ*.

3.5. Zebrafish imaging

Given the selective LDs imaging of **CMDP** derivatives, we chose zebrafish as the experimental model to explore **CMDP** derivatives' imaging capability *in vivo*. Three days after fertilization, the yolk sac has lots of neutral lipids that provides energy for

zebrafish larval growth, seeing it is an ideal model for researching the lipid-associated diseases [22-25]. The zebrafish were observed after incubated with **CMDP-CN** and **CMDP-NO₂** for 15 mins and were imaged rapidly via CLSM. As shown in **Fig. 6**, intense yellow and red fluorescent signals were basically originated from zebrafish. Hence, the above imaging outcome indicated that **CMDP-CN** and **CMDP-NO₂** can stain zebrafish, which had huge possibility in detecting lipid production and consumption.

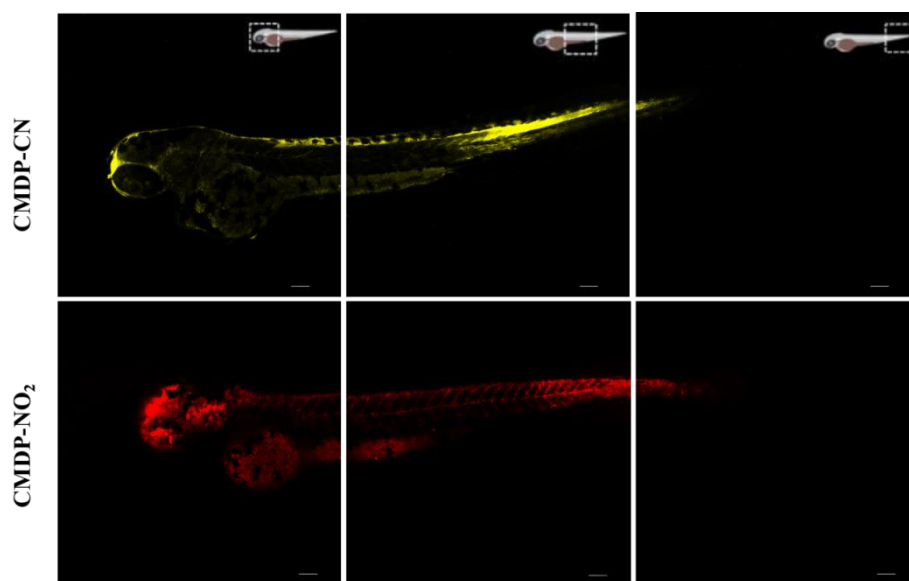


Fig. 6. Confocal images of zebrafish stained with **CMDP-CN** and **CMDP-NO₂** (5.0 μ M). Scale bar: 100 μ m.

4. Conclusion

In conclusion, we constructed a series of novel AIEgens through a facile hybridization of naphthalenone and phenyl acetonitrile with different substituents. The AIE property of the **CMDP** derivatives was put down to effective inhibition of RIR in the aggregation state. Because of the unique AIE nature and the appropriate lipophilicities, **CMDP-CN** and **CMDP-NO₂** could characteristically stain LDs in cells even without washing. Moreover, *in vivo* staining of zebrafish was also obtained by employing **CMDP** derivatives. This study not only provided a simple strategy to construct functionalized AIEgens, but also enlarged their bio-imaging applications for lipid.

Acknowledgements

The authors thank the National Natural Science Foundation of China (No. 21572177), the International Science & Technology Cooperation Program of Shaanxi Province (No. 2019KWZ-001), Biomedicine Key Laboratory of Shaanxi Province (No. 2018SZS41).

References

- [1] Jin Y, Ren ZQ, Tan YJ, Zhao PX, Wu J. Motility plays an important role in the lifetime of mammalian lipid droplets. *Int J Mol Sci* 2021; 22: 1-11.
- [2] Olzmann JA, Carvalho P. Dynamics and functions of lipid droplets. *Nat Rev Mol Cell Bio* 2019; 20: 137-155.
- [3] Thiam AR, Beller M. When and how of lipid droplet diversity. *J Cell Sci* 2017; 130: 315-324.
- [4] (a) Ning YY, Cui JH, Lu YW, Wang XQ, Xiao CN, Wu SP, Li JL, Zhang YM. De novo design and synthesis of a novel colorimetric fluorescent probe based on naphthalenone scaffold for selective detection of hypochlorite and its application in living cells. *Sensor Actuat B-Chem* 2018; 269: 322-330; (b) Ning YY, Wang XQ, Sheng KJ, Yang LL, Xiao CN, Li JL, Zhang YM, Wu SP. A novel colorimetric and fluorescence turn-on pH sensor with a notably large Stokes shift for its application. *New J Chem* 2018; 42: 14510-14516.
- [5] (a) Wang Z, He XW, Yong TY, Miao Y, Zhang C, Tang B. Multicolor tunable polymeric nanoparticle from the tetraphenylethylene cage for temperature sensing in living cells. *J Am Chem Soc* 2020; 142: 512-519; (b) Shi DL, Liu WW, Wang GW, Guo Y, Li J. Small-molecule fluorescence-based probes for aging diagnosis. *Acta Materia Medica* 2022; 1: 4-23.
- [6] (a) Wang KN, Liu LY, Mao D, Xu SD, Tan CP, Cao Q, Mao ZW, Liu B. A polarity-sensitive ratiometric fluorescence probe for monitoring changes in lipid droplets and nucleus during ferroptosis. *Angew Chem Int Ed* 2021; 60: 15095-15100; (b) Zhao Q, Sun Z. Red and near infrared emission materials with AIE characteristics. *J Mater Chem C* 2016; 4: 10588-10609.
- [7] Wang D, Su HF, Kwok RT, Shan GG, Leung AC, Lee MM, Sung HH, Williams ID, Lam JW, Tang BZ. Facile synthesis of Red/NIR AIE luminogens with simple structures, bright emissions, and high photostabilities, and their applications for specific imaging of lipid droplets and image-guided photodynamic therapy. *Adv Funct Mater* 2017; 27: 1-10.
- [8] (a) Sturala J, Etherington MK, Bismillah AN, Higginbotham HF, Trewby W, Aguilar JA, Bromley EH, Avestro AJ, Monkman AP, McGonigal PR. Excited-state aromatic interactions in the aggregation-induced emission of molecular rotors. *J Am Chem Soc* 2017; 139: 17882-17889; (b) Liu CH, Zhou L, Xie LJ, Zheng Y, Man HZ, Xiao Y. Forthrightly monitoring ferroptosis induced by endoplasmic reticulum stresses through fluorescence lifetime imaging of microviscosity increases with a specific rotor. *Chinese Chem Lett* 2022; 33: 2537-2540; (c) Zhang XF, Wang L, Li N, Xiao Y. Assessing chromatin condensation for epigenetics with a DNA-targeting sensor by FRET and FLIM techniques. *Chinese Chem Lett* 2021; 32: 2395-2399.
- [9] (a) Yao Z, Zhang BS, Steinhardt RC, Mills JH, Prescher JA. Multicomponent bioluminescence imaging with a pi-extended luciferin. *J Am Chem Soc* 2020; 142: 14080-14089; (b) Yue XX, Xu J, Liu XZ, Song XZ, Foley JW. Improved synthetic method of Benzo[a]phenoselenazinium phototherapeutic agents. *Dyes Pigm* 2021; 188: 1-6. (c) He TJ, Adam CS, Han HH, Sen Sj, Chen GR, Zang Y, Jonathan LS, Tony DJ, Li J, He XP. Fluorescent probes for the imaging of lipid droplets in live cells. *Coord Chem Rev* 2021; 427: 1-14. (d) Xiao HB, Li P, Tang B. Recent progresses in fluorescent probes for detection of polarity. *Coord Chem Rev*

- 2021; 427: 1-32.
- [10] (a) Tian GJ, Sun DX, Zhang YG, Yu X. Franck-condon blockade and aggregation-modulated conductance in molecular devices using aggregation-induced emission-active molecules. *Angew Chem Int Ed* 2019; 58: 5951-5955; (b) Han JJ, Lee HW, Chen YH, Li HD, Kim HM, Yoon J. Observing hepatic steatosis with a commercially viable two-photon fluorogenic probe. *Mater Chem Front* 2022; 6: 553-560. (c) Ren XJ, Liao LD, Yang ZG, Li HP, Li X, Wang YG, Ye Y, Song XZ. Rational design of a bifunctional fluorescent probe for distinguishing Hcy/Cys from GSH with ideal properties. *Chin Chem Lett* 2021; 32: 1061-1065.
- [11] Wang D, Tang BZ. Aggregation-induced emission luminogens for activity-based sensing. *Accounts Chem Res* 2019; 52: 2559-2570.
- [12] Zhao N, Ma CC, Yang WY, Yin W, Wei JH, Li N. Facile construction of boranil complexes with aggregation-induced emission characteristics and their specific lipid droplet imaging applications. *Chem Commun* 2019; 55: 8494-8497.
- [13] Fan L, Wang XD, Zan Q, Zhou R, Wang CG, Yan X, Jia XT, Liu XM, Gao Y, Wang LJ, Lu GY. Lipid droplet-specific fluorescent probe for in vivo visualization of polarity in fatty liver, inflammation, and cancer models. *Anal Chem* 2021; 93: 8019-8026.
- [14] Yin W, Li Y, Li N, Yang WY, An H, Gao JR, Bi Y, Zhao N. Hybridization of triphenylamine and salicylaldehyde: A facile strategy to construct aggregation-induced emission luminogens with excited-state intramolecular proton transfer for specific lipid droplets and gram-positive bacteria imaging. *Adv. Optical Mater* 2020; 8: 1-10.
- [15] Song CW, Tamima U, Reo YJ, Dai M, Sarkar S, Ahn KH. A rationally designed polarity-viscosity sensitive probe for imaging lipid droplets. *Dyes Pigments* 2019; 171: 1-13.
- [16] Wu MY, Leung JK, Kam C, Chou TY, Wang D, Feng S, Chen SJ. A near-infrared AIE probe for super-resolution imaging and nuclear lipid droplet dynamic study. *Mater Chem Front* 2021; 5: 3043-3049.
- [17] Ni JS, Liu HX, Liu JK, Jiang MJ, Zhao Z, Chen YC, Kwok RT, Lam JW, Peng Q, Tang B. The unusual aggregation-induced emission of coplanar organoboron isomers and their lipid droplet-specific applications. *Mater Chem Front* 2018; 2: 1498-1507.
- [18] Liu GN, Peng GS, Dai JA, Zhou R, Wang CG, Yan X, Jia XT, Liu XM, Gao Y, Wang LJ, Lu GY. STED nanoscopy imaging of cellular lipid droplets employing a superior organic fluorescent probe. *Anal Chem* 2021; 93: 14784-14791.
- [19] Ye MT, Hu W, He M, Zhai SY, Liu ZH, Wang YY, Zhang HJ, Li CY. Deep imaging for visualizing nitric oxide in lipid droplets: discovering the relationship between nitric oxide and resistance to cancer chemotherapy drugs. *Chem Commun* 2020; 56: 6233-6236.
- [20] Guo R, Yin JL, Ma YY, Li GH, Wang Q, Lin WY. A novel NIR probe for detection of viscosity in cellular lipid droplets, zebra fishes and living mice. *Sensor Actuat B-Chem* 2018; 271: 321-328.
- [21] Yu CJ, Fang XB, Wang H, Guo X, Sun LL, Wu QH, Jiao LJ, Hao EH. A family of highly fluorescent and membrane-permeable bis(BF₂) acyl-pyridinylhydrazine dyes with strong solid-state emission and large stokes shifts: The BOAPH fluorophores. *J Org Chem* 2021; 86: 11492-11501.
- [22] Zheng X, Zhu W, Ni F, Ai H, Gong S, Zhou X, Sessler JL, Yang C. Simultaneous dual-colour tracking lipid droplets and lysosomes dynamics using a fluorescent probe. *Chem Sci* 2019; 10:2342-2348.

- 316 [23] Artola M, Kuo CL, Lelieveld LT, Rowland RJ, Marel GA, Codee JD, Boot RG, Davies GJ,
317 Overkleeft HS. Functionalized cyclophellitols are selective glucocerebrosidase inhibitors and
318 induce a bona fide neuropathic gaucher model in zebrafish. *J Am Chem Soc* 2019; 141: 4214-
319 4218.
- 320 [24] Kooij R, Liu SH, Sapmaz A, Xin BT, Janssen GM, van Veelen PA, Ovaa H, ten Dijke P,
321 Geurink PP, Small-molecule activity-based probe for monitoring ubiquitin C-terminal
322 hydrolase L1 (UCHL1) activity in live cells and zebrafish embryos. *J Am Chem Soc* 2020;
323 142:16825-16841.
- 324 [25] Breuer M, Patten SA. A great catch for investigating inborn errors of metabolism-insights
325 obtained from zebrafish. *Biomolecules* 2020; 10: 1-24.